

See discussions, stats, and author profiles for this publication at: <https://www.researchgate.net/publication/262696237>

# Energetics and Solvation Structure of a Dihalogen Dopant ( $I_2$ ) in He-4 Clusters

ARTICLE *in* THE JOURNAL OF PHYSICAL CHEMISTRY A · MAY 2014

Impact Factor: 2.69 · DOI: 10.1021/jp502994g · Source: PubMed

---

CITATION

1

READS

36

## 4 AUTHORS, INCLUDING:



Ricardo Pérez de Tudela

Ruhr-Universität Bochum

31 PUBLICATIONS 201 CITATIONS

[SEE PROFILE](#)



Patricia Barragán

17 PUBLICATIONS 284 CITATIONS

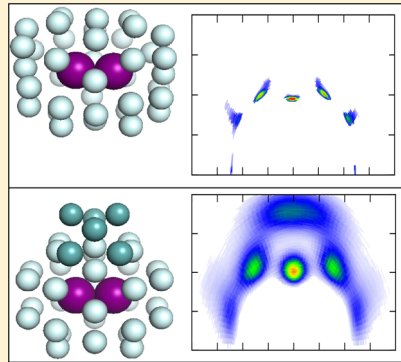
[SEE PROFILE](#)

# Energetics and Solvation Structure of a Dihalogen Dopant ( $I_2$ ) in $^4He$ Clusters

Ricardo Pérez de Tudela,<sup>†</sup> Patricia Barragán,<sup>‡</sup> Álvaro Valdés,<sup>§</sup> and Rita Prosmiti\*

Instituto de Física Fundamental (IFF-CSIC), CSIC, Serrano 123, 28006 Madrid, Spain

**ABSTRACT:** The energetics and structure of small  $He_NI_2$  clusters are analyzed as the size of the system changes, with  $N$  up to 38. The full interaction between the  $I_2$  molecule and the He atoms is based on analytical *ab initio* He– $I_2$  potentials plus the He–He interaction, obtained from first-principle calculations. The most stable structures, as a function of the number of solvent He atoms, are obtained by employing an evolutionary algorithm and compared with CCSD(T) and MP2 *ab initio* computations. Further, the classical description is completed by explicitly including thermal corrections and quantum features, such as zero-point-energy values and spatial delocalization. From quantum PIMC calculations, the binding energies and radial/angular probability density distributions of the thermal equilibrium state for selected-size clusters are computed at a low temperature. The sequential formation of regular shell structures is analyzed and discussed for both classical and quantum treatments.



## I. INTRODUCTION

van der Waals (vdW) complexes of dihalogen molecule surrounded by several rare gas atoms have been intensely studied over the past decades by high resolution spectroscopy techniques.<sup>1–6</sup> They are size-selected spectroscopically identified by a band shift in the halogen molecule ( $B,\nu \leftarrow (X,\nu'=0)$ ) spectra for each additional rare gas atom in the complex.<sup>2,7</sup> Thus, for the smaller complexes incorporating one or two rare gas atoms, spectroscopy in the visible region involving an electronic  $B \leftarrow X$  transition<sup>2,5–8</sup> offers the possibility of a detailed comparison with the theory.<sup>9–15</sup> In this case, an accurate description of the intermolecular forces through the relevant electronic potential energy surfaces,<sup>13,16,17</sup> and also of the photopredissociation dynamics and energy redistribution mechanisms have been addressed.<sup>2,4,5,7,10–12,18,19</sup>

Additionally, interest in species containing He atoms has intensified in recent years owing to the development of methods to synthesize and characterize doped helium nanodroplets<sup>20–24</sup> and have led to numerous computational efforts to simulate their properties (refs 25–32 and references therein). Clusters are used as model microsolutions to understand the transition from the gas to condensed phase. Despite their relatively small size, clusters retain many characteristics of the bulk and they are theoretically tractable, although they are sufficiently complex to be a useful approach and a great simplification to more complicated systems.

In the present work, we intend to show how a simple dihalogen molecule inside a series of small He clusters provides us with microscopic information on the structuring, which can realistically describe its dependence on features/properties of more complicated larger systems. The  $I_2$  is a very heavy molecule, and its interaction potential with He atom is quite anisotropic, presenting a double-minima topology at linear He–I–I and T-shaped He– $I_2$  configurations.<sup>13</sup> Moreover, on

the basis of recent *ab initio* data,<sup>13</sup> the energy difference between these two potential wells is very close to the He–He interaction of  $-7.62\text{ cm}^{-1}$  at its equilibrium distance. In particular, the global minimum (linear) of the  $HeI_2$  cluster is at an energy value of  $-44.28\text{ cm}^{-1}$ , and the second one (T-shaped) is at  $-38.92\text{ cm}^{-1}$ , which is higher in energy by only  $5.36\text{ cm}^{-1}$ , and the barrier between them is at an energy of  $-18.43\text{ cm}^{-1}$ . By considering now a growth sequence from  $He-I_2$  to larger  $He_NI_2$  clusters as  $N$  increases, we can conceive various scenarios based on the balance of the linear and T-shaped  $He-I_2$  potential interactions with He–He ones. However, for highly anharmonic quantum systems zero-point energy (ZPE) effects should be considered if we desire to rule out a reliable scenario on the structuring of these clusters. More specifically, for the triatomic  $HeI_2$  complex by including the quantum zero-point energy a difference of only  $0.2\text{ cm}^{-1}$  has been obtained between the linear and T-shaped conformers.<sup>13</sup> On the contrary, for the tetraatomic  $He_2I_2$ , the ZPE effects win over the potential, and the order of the quantum structures are the reverse of that of the classical ones.<sup>33</sup> As expected, the potential surface plays an important role; however, we cannot, *a priori*, distinguish on the structuring and energetics of such complexes, based only on the energy landscape without further explicit nuclear computations.<sup>34,35</sup>

Our study deals with the characterization of the small clusters where, as an initial simple example, a single  $I_2$  molecule is embedded in the He droplet. We shall therefore start by using the CCSD(T)/CBS[Q5] (coupled-cluster at complete basis set limit) potential energy surface (PES) between the  $I_2$  molecule

**Special Issue:** Franco Gianturco Festschrift

**Received:** March 26, 2014

**Revised:** May 27, 2014

**Published:** May 28, 2014

and a single He atom<sup>13</sup> as the basis for a sum-of-potentials scheme, and then, we shall first check how we can reproduce the interaction potential for the smaller species. For example, for the  $\text{He}_2\text{I}_2$  system, it has been shown that such a potential form represents very accurately the PES of this system.<sup>33</sup> Therefore, *ab initio* calculations were performed for such comparison for selected larger complexes. In turn, we employ a genetic algorithm to locate their potential minima, and then we use classical Monte Carlo (MC) and quantum path integral Monte Carlo (PIMC) approaches. In this way, we obtained structural information and quantitative estimates of the involved energetics and of the ensuing geometric features at the quantum level at low temperature, comparable to the experimental ones for these systems.<sup>6,11</sup>

The paper is organized as follows: the next section describes the computational methods and tools employed to obtain both the potential surfaces and the quantum observables, whereas in section III we present and discuss the results obtained for the structures and energetics of the  $\text{I}_2$  molecule surrounded by He of varying size up to 38 atoms. Section IV will finally give our present conclusions.

## II. COMPUTATIONAL METHODS AND DETAILS

### A. Modeling of the Interaction: *Ab Initio* Calculations.

On the basis of our previous studies on larger  $\text{He}_n$ -dihalogen molecule complexes<sup>14,15,33,35</sup> we choose to represent the analytical PES of  $\text{He}_N\text{I}_2$  as the sum of the three-body parametrized  $\text{HeI}_2$  interactions plus the He–He interaction,

$$V(\vec{R}_i, r_e) = \sum_i V_{\text{HeI}_2}(\vec{R}_i, r_e) + \sum_{il} V_{\text{HeHe}}(\vec{R}_{il}) \quad (1)$$

where the corresponding  $V_{\text{HeI}_2}(\vec{R}_i, r_e)$  terms are the CCSD(T)/CBS parametrized  $V_{\text{HeI}_2}(R_i, \theta_i, r_e)$  potential of the  $\text{HeI}_2$  complex of ref 13 and  $V_{\text{HeHe}}(\vec{R}_{il})$  is the potential function for  $\text{He}_2$  given in ref 36. The equilibrium ground state  $\text{I}_2$  bond length is  $r_e = 2.666 \text{ \AA}$ , the  $\vec{R}_i$  are the vectors connecting the center of mass of  $\text{I}_2$  with each He atom, and  $\theta_i$  are the angles between each  $\vec{R}_i$  vector and the  $\text{I}_2$  axis. The resulting analytical surface is evaluated by carrying out *ab initio* electronic structure calculations at selected geometries of different  $\text{He}_N\text{I}_2$  clusters, e.g.,  $N = 3–10, 21, 26, 32$ , and 38 ones. Specifically, single-point, optimization, and frequency analysis calculations at CCSD(T) and/or MP2 levels of theory are carried out using large-core, such as the ECP46MWB,<sup>37</sup> effective core potentials (ECP) for iodine atoms, whereas large basis sets, such as augmented correlation-consistent polarized basis sets<sup>38</sup> aug-cc-pVQZ (AVQZ), were used for He atoms, depending of the size of the system. The *ab initio* calculations are performed using the Gaussian<sup>39</sup> and Molpro<sup>40</sup> packages. The interaction energies are computed within the supermolecular approach,  $\Delta E = E_{\text{He}_N\text{I}_2} - \sum_{i=1}^N E_{\text{He}_i}^{\text{BSSE}} - E_{\text{I}_2}^{\text{BSSE}}$ , and all energy values are corrected for the BSSE effect with the usual counterpoise procedure of Boys and Bernardi.<sup>41</sup>

**B. Evolutionary Algorithm.** To locate the equilibrium configurations (global or local minima) on the PES, we employed an evolutionary algorithm (EA).<sup>42</sup> Such a procedure provides a reasonably fast way to find minima of a general function, and in particular it has been proven to be well suited for atomic clusters based on pair interactions. Details of the implementation can be found in ref 42. Briefly, one considers

an initial population of  $M$  individuals ( $\text{He}_N\text{I}_2$  clusters in our case). This population is characterized by two sets of vectors:  $\vec{x}_i$  and  $\vec{\eta}_i$ , with  $i = 1, \dots, M$ , which contain, respectively, the Cartesian coordinates and the strategy parameters of all the individuals. The latter controls the evolution of the dispersion of the population in time. The initial population is created with random values for  $x_i$  and  $\eta_i = 1$  in the interval  $(0, \Delta)$ , with  $\Delta$  being a displacement factor that increases the resolution power. This first parent set evolves to generate a new population according to the following evolution law:

$$x'_i(j) = x_i(j) + \eta_i(j) N_j(0,1) \quad (2)$$

$$\eta'_i(j) = \eta_i(j) \exp[\tau' N(0,1) + \tau'' N_j(0,1)] \quad (3)$$

where  $N(0,1)$  is a Gaussian random number of average zero and standard deviation 1.  $N_j(0,1)$  indicates that the random number is generated for each  $j = 1 – 3N$  coordinates, and  $\tau'$  and  $\tau''$  are adjustable parameters of the method. For each individual of the joint parent-child group ( $2M$  individuals)  $q$  opponents are randomly chosen to *fight* each other, and the individual in each encounter with the lower potential energy wins. The best  $M$  individuals then become parents for the next generation and so on. Convergence is achieved when the potential energy difference between two consecutive generations is below a threshold value.

**C. PIMC Approach.** For the  $\text{He}_N\text{I}_2$ , with  $N = 8–38$ , complexes we adopt here the quantum PIMC formalism.<sup>43</sup> This is a quantum-statistical nature treatment, going beyond a standard harmonic frequency analysis, and has been applied to derive temperature-dependent properties of molecular systems.<sup>44</sup> Briefly, to compute the thermal average of the property  $\mathcal{A}$ , the following expression must be evaluated:

$$\langle \mathcal{A} \rangle = Z^{-1} \int dX dX' \rho(X, X'; \beta) \langle X | \mathcal{A} | X' \rangle \quad (4)$$

where  $Z = \int dX \rho(X, X; \beta)$  is the partition function and  $\rho(X, X'; \beta) = \langle X | e^{-\beta \hat{H}} | X' \rangle$  is the density matrix of the system at a temperature  $T = 1/k_B \beta$ , with  $X$  being a  $3N$ -dimensional vector containing the Cartesian coordinates of all the helium atoms and  $\hat{H} = \hat{K} + \hat{V} = -(\hbar^2/2m_{\text{He}})\sum_{i=1}^N \nabla_i^2 - (\hbar^2/2m_{\text{I}_2})\nabla_{\text{I}_2}^2 + V(\vec{R}_i, r_e)$  being the Hamiltonian of the whole system.

The path integral Monte Carlo method<sup>45</sup> makes use of a convolution property that allows the density matrix of a quantum system of  $N$  particles at a temperature  $T$  to be computed as a multidimensional integral of the product of  $M$  density matrices at a higher temperature  $MT$ :

$$\begin{aligned} &\rho(X, X'; \beta) \\ &= \int dX_1 \dots dX_{M-1} \rho(X, X_1; \beta/M) \dots \rho(X_{M-1}, X'; \beta/M) \end{aligned} \quad (5)$$

Several approximations<sup>46,47</sup> can be made in these new  $\rho(X, X_i; \beta/M)$  density matrices, the most trivial being the so-called *primitive approximation*, where the commutator between the kinetic and the potential operators is neglected, which leads to a complete separation between kinetic  $\rho_{\text{free}}$  and potential  $\rho_V$  density matrices:

**Table 1.** Potential Energy Values (EA-Opt) for the Three Lower Optimal Structures Predicted by the Evolutionary Algorithm for the Indicated  $\text{He}_N\text{I}_2$  Clusters Using the PES of Eq 1<sup>a</sup>

N	global minimum			local minimum-1	local minimum-2
	EA-Opt/CCSD(T) PES/AVQZ	MP2-Opt AVTZ	CCSD(T) AVTZ/AVQZ	EA-Opt PES	
3	-132.32/-127.13	-96.68	-109.36/-127.33	-130.23	-128.17
4	-179.22/-172.24	-132.17	-149.46/-172.33	-177.21	-174.99
5	-226.15/-217.40	-165.34	-188.22/-217.78	-224.24	-222.11
6	-273.16/-262.63	-197.20	-226.73/-264.13	-271.32	-269.28
7	-320.59/-308.28	-231.51	-266.44/-310.05	-318.46	-316.49
8	-374.87/-360.44	-268.56	-312.53/-362.51	-366.03	-363.67
9	-420.44/-406.31	-306.44	-353.02/-408.33	-411.43	
global minimum			local minimum-1		local minimum-2
EA-Opt/MP2 PES/AVTZ[AVDZ]			local minimum-1		local minimum-2
10	-466.01/-273.81	-344.22	-390.15/-		
21	-983.94/-491.93	-667.39			
26	-1207.08/-586.43				
32	-1509.37/-718.37				
38	-1769.66/-757.3 3			-1760.07	

<sup>a</sup>Ab initio interaction energies from MP2/AVTZ optimizations and single point CCSD(T) calculations at both optimal predicted structures up to  $N = 10$  are also listed, whereas for the larger clusters  $N = 21, 26, 32$ , and 38 MP2 results are given. The large-core ECP46MWB ECP is employed for the I atoms, and AVTZ or AVQZ basis sets are used for both I and He atoms or AVTZ for I and AVDZ for He atoms (AVTZ[AVDZ]). The corresponding spatial arrangements of them are shown in Figures 2 and 3. Energies are in  $\text{cm}^{-1}$ .

$$\rho_{\text{free}}(X_i, X_j; \beta/M) = \left( \frac{4\pi\hbar^2\beta}{2mM} \right)^{-3N/2} \exp\left[ -\frac{2mM}{4\hbar^2\beta} (X_i - X_j)^2 \right]$$

$$\rho_V(R_i, R_j; \beta/M) = \delta(X_i - X_j) e^{-(\beta/M)V(X_i)} \quad (6)$$

The multidimensional integrals involved in eq 4 are carried out using the Monte Carlo method that samples the configurational space following a probability density function defined as the product of the density matrices in eq 4. A particularly effective sampling technique called *staging*<sup>48</sup> is used to perform smart collective bead movements (within the classical isomorphism) that directly sample the kinetic part, using a Metropolis<sup>49</sup> algorithm for the potential part. We checked two fundamentally different kinetic energy estimators (thermodynamic and virial ones),<sup>50,51</sup> and both of them yield almost identical values. We found that the virial estimator tends to converge faster than the one proposed by Barker,<sup>50</sup> and also exhibits smaller deviation, and thus we employed this in the present calculations.

### III. RESULTS AND DISCUSSION

**A. Optimal Potential Energy Configurations.** Using the EA optimization procedure for the potential surface of eq 1, we compute the different minima for the  $\text{He}_N\text{I}_2$  clusters, with  $N = 1\text{--}38$ . The energy convergence threshold was chosen to be  $0.0001 \text{ cm}^{-1}$ , and the potential energy values for the three lowest minima (namely global, local-1, and local-2) for the clusters with  $N = 2$  up to 9 He atoms are given in Table 1. We found that for all these clusters the energies of their three minima lie very close with differences of 2 and  $4 \text{ cm}^{-1}$ , respectively, up to the  $N = 7$  cluster, whereas for the  $N = 8$  one an energy difference of  $8.84 \text{ cm}^{-1}$  is obtained between its global and local-1 minima. In turn, in Figure 1 we plot the minimum

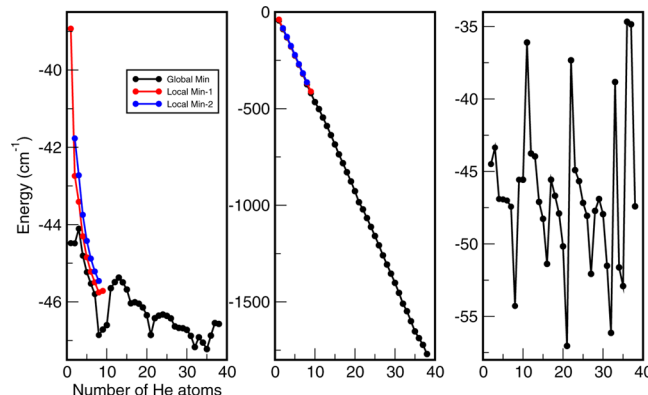


**Figure 1.** Average energy per He atom, total potential minimum energy, and classical evaporation energy,  $E_N - E_{N-1}$ , as a function of the number of He atoms for the  $\text{He}_N\text{I}_2$  clusters with  $N = 1\text{--}38$ .

energy per He atom (left panel), the total potential minimum energy (middle panel), and the classical evaporation energy  $E_N - E_{N-1}$  for  $N > 1$  (right panel). One can see that the total energy is decreasing as the number of He atoms increases. The first marked change occurs for  $N = 8$ , where the average energy per He atom and the classical evaporation energy are significantly reduced with respect to that of the previous ones. A similar behavior is also found for the  $N = 21$  and  $N = 32$  clusters. We should note that the average energy per particle, in all the clusters studied, is very similar. Although the He–I<sub>2</sub> interaction is stronger than that of the He–He, the latter cannot be neglected. The explanation for the similarity in the energies per particle comes from the fact that the energy difference between the two equilibrium (linear and T-shaped) configurations in HeI<sub>2</sub>, as we mentioned above, is very close to the He–He interaction. In particular, this difference counts to  $5.36 \text{ cm}^{-1}$  and the He–He well depth is  $7.62 \text{ cm}^{-1}$ .

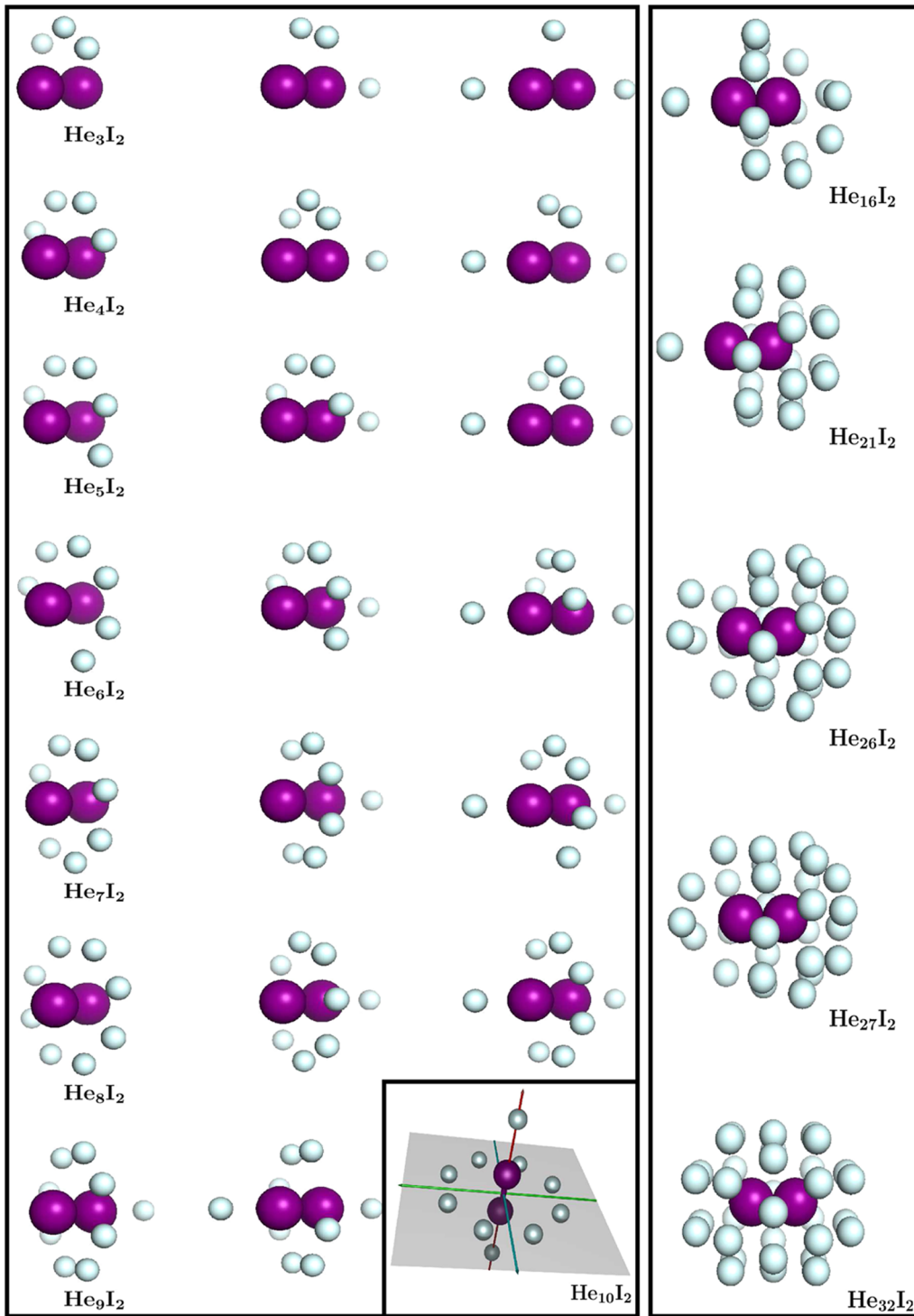


**Figure 2.** Optimal structures of the indicated  $\text{He}_N\text{I}_2$  obtained from the EA on the analytical PES of eq 1, with  $N = 3\text{--}9$  (left panel), for the lowest energy configurations, global (left column), local minimum-1 (middle column), and local minimum-2 (right column), for the global minimum of the  $\text{He}_{10}\text{I}_2$  (inset plot of the left panel), and for  $N = 16, 21, 26, 27$ , and 32 clusters (right panel).

In the left panel of Figure 2 the spatial arrangements for the global (left column) as well as the two local minima, namely, local-1 (middle column) and local-2 (right column), for each of the  $\text{He}_N\text{I}_2$  clusters with  $N \leq 10$  are displayed. As can be seen, the helium atoms in these clusters can be placed either in the linear configurations or in the perpendicular (T-shaped) to the  $\text{I}_2$  axis forming a ring. As we mentioned above, the global minimum of the  $\text{He}_2\text{I}_2$  surface is found to be for a linear configuration, whereas for the  $\text{He}_3\text{I}_2$  up to  $\text{He}_8\text{I}_2$  clusters a sort

of ring-like arrangement is enveloping around the  $\text{I}-\text{I}$ . These structures are the most favorable energetically, and the completion of the first ring at  $N = 8$  is also signaled by the marked change in the average and evaporation energy, as indicated in Figure 1. This central ring, which is fully completed with 8 He atoms, constitutes a skeleton for larger clusters, as we will discuss later. The structure in the inset plot of the left panel of Figure 2 shows the optimal configuration for the  $\text{He}_{10}\text{I}_2$  cluster, with the two next He atoms be placed in linear

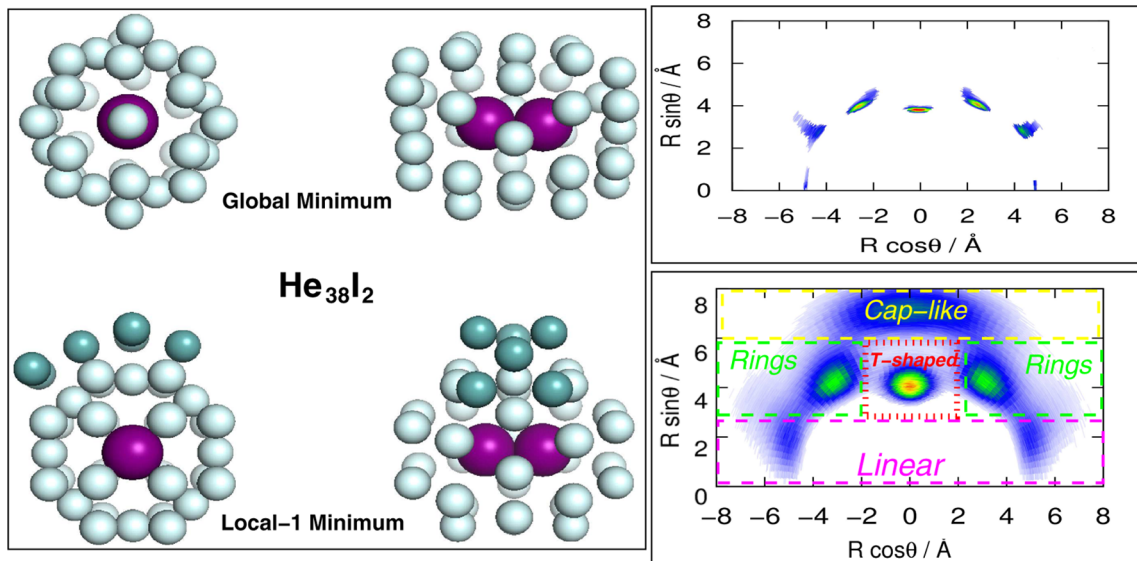


**Figure 3.** Two lowest energy structures on the PES of the  $\text{He}_{38}\text{I}_2$  cluster (top and side view in the left panel) and the corresponding classical (right top panel) and quantum (right bottom panel) 2D distributions from the PIMC calculations. The marked areas correspond to the spatial regions used in the partial integrations (see text).

arrangements. This trend clearly follows the characteristics of the underlying PES. As we mentioned above, the difference in energy between the linear and the T-shape wells for the  $\text{He}_2\text{I}_2$  trimer is smaller than the interaction energy between two He atoms, thus they prefer to stick together in the central ring, until it is completely full, and afterward they occupy the two linear ones.

For clusters with  $N > 10$ , He atoms continue surrounding the  $\text{I}_2$  molecule, filling the gaps between the central ring and the atoms placed at the linear arrangements. In particular, the optimal structures of five selected size clusters ( $N = 16, 21, 26, 27, 32$ ) are shown in the right panel of Figure 2. The choice of these structures corresponds to different steps in the solvation process. For  $\text{He}_{16}\text{I}_2$ , the He atoms 11–14 and 15–16 gather along two rings located in the one-side of the central one, with a reordering of the He atoms that blurs the description in terms of completed rings. In the  $\text{He}_{21}\text{I}_2$  cluster we observe the completion of these two additional rings that shows the solvation of one of the I atoms, whereas for  $N = 26$  and  $N = 27$  we can follow the filling of the rings in the other side. In turn, the solvation of the  $\text{I}_2$  molecule continues until it is completed with  $N = 32$  He atoms in the cluster, forming five rings around the molecule. We can check in Figure 1 that the most stable structures are  $N = 8$  (central ring filled),  $N = 21$  (solvation of one I atom), and  $N = 32$  (complete first solvation shell around the  $\text{I}_2$  molecule), showing marked minima in either the energy per atom or the evaporation energy graphs.

In Figure 3 we show top and side views of the two lowest in energy configurations for the  $\text{He}_{38}\text{I}_2$  cluster, left top and bottom panels, respectively. The energy difference between them counts for  $9.6 \text{ cm}^{-1}$ , and as can be seen, the lower arrangement (left top panels) corresponds to a five-ring configuration plus two He atoms in linear ones, whereas in the next (left bottom panels) the six He atoms formed a cup-like structure around the  $\text{He}_{32}\text{I}_2$  cluster, or a second solvation shell around the  $\text{I}_2$  molecule.

To check the analytical representation of the PES (eq 1), we performed MP2 and CCSD(T) calculations for different size clusters, and we list these results in Table 1. As we mentioned

before, the analytical PESs for the clusters are based on the triatomic CCSD(T)/ECP28MDF/CBS[Q5] data,<sup>13</sup> however, as the size of the cluster increases, computation at such levels of theory and basis sets becomes a prohibitive task, and thus we are limited here to CCSD(T) and MP2 data. Further, it has been shown<sup>33</sup> that for the  $\text{He}_2\text{I}_2$  cluster, the CCSD(T)/ECP28MDF/AVQZ results are within about  $10 \text{ cm}^{-1}$  higher in energy with respect to their CBS[Q5] extrapolation, whereas the MP2 and CCSD(T) energies using the large-core ECP46MWB and AVQZ basis sets are by about 15 and 5  $\text{cm}^{-1}$ , respectively, higher in energy with respect the above CBS[Q5] limit. Thus, such finding for the  $\text{He}_2\text{I}_2$  system serves here as indicator for the accuracy of CCSD(T) and MP2 methodologies using smaller basis sets for larger clusters.

The potential energy values for the smaller  $\text{He}_N\text{I}_2$  clusters, with  $N$  up to 10, at the global minimum configuration are compared with the interaction energies obtained by *ab initio* MP2/AVTZ optimization calculations, and with single-point ones at the CCSD(T) level of theory using both AVTZ and AVQZ basis sets with the ECP46MWB effective core potential (ECP) for the I atoms. Optimal structures obtained by minimization of the analytical PES and by optimization at the MP2 level, are found to be very similar to each other (e.g., see those displayed in Figure 2). The calculated MP2 energies show differences, compared to the analytical form, up to  $127 \text{ cm}^{-1}$  for the  $\text{He}_{10}\text{I}_2$ , although their corresponding CCSD(T) values are closer to the ones predicted by the analytical PES (Table 1) within  $80$  and  $15 \text{ cm}^{-1}$  using the AVTZ and AVQZ basis sets, respectively. In Table 1 we also list the optimal energies for the larger  $\text{He}_{21}\text{I}_2$ ,  $\text{He}_{26}\text{I}_2$ ,  $\text{He}_{32}\text{I}_2$ , and  $\text{He}_{38}\text{I}_2$  clusters predicted by the analytic potential (eq 1), together with MP2 electronic structure calculations. One can see that the obtained energy differences should be attributed to the rather small basis set (AVTZ[AVDZ]) employed in these calculations, as we mentioned above. For clusters with  $N$  up to 10 the analytical PES predicts values in close agreement with the *ab initio* computed CCSD(T) interaction energies, whereas for the larger systems the obtained differences are attributed to the effect of the MP2 method and basis set employed. Overall, we

may say that the sum-of-potentials analytical approach adopted here represents reasonable well the topology of the underlying PES of these systems.

**B. Thermal Equilibrium Energies and Structures: Classical and Quantum Calculations.** To compute the thermal equilibrium states and investigate the effect of nuclear quantum effects for these clusters, we carried out classical MC and PIMC simulations. The global minimum configurations obtained from the evolutionary algorithm were used as the starting points in the these calculations. The number of MC steps was adjusted in each case so that each degree of freedom were sampled at least  $10^4$  times. We have carried out calculations with different number of beads  $M = 1, 10, 50, 100, 200$ , and  $300$ ,  $M = 1$  being the classical MC simulations. To obtain the energy in the  $M \rightarrow \infty$  limit, a quadratic extrapolation of the type  $a + b\tau^2$  was made,<sup>26</sup> where  $\tau = 1/M$  and  $a, b$  are the parameters. In Figure 4 we plot the

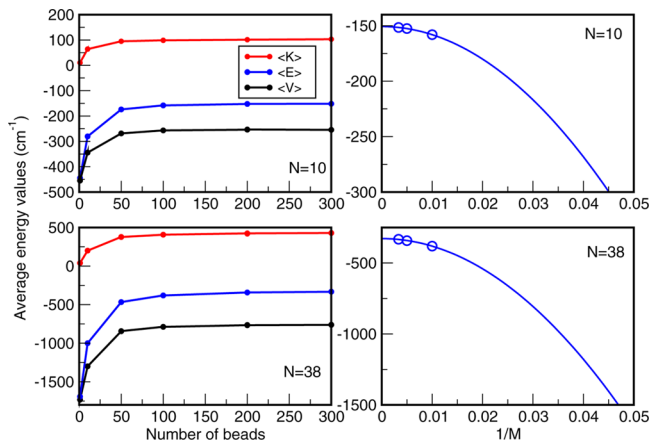


**Figure 4.** Convergence of kinetic, potential, and total energy as a function of the number of beads ( $M$ ) (left panels), and extrapolation of the total energy in the  $M \rightarrow \infty$  limit (right panels) from the PIMC simulations for  $\text{He}_N\text{I}_2$  with  $N = 10$  and  $38$  at  $T = 1 \text{ K}$ .

convergence tests for kinetic, potential, and total energy made for the  $N = 10$  and  $38$  clusters. One can see in the left panel of Figure 4 that values obtained with  $M = 100, 200$ , and  $300$  are fully converged, and we only considered these energies in the quadratic fit for computing the total energy at  $M \rightarrow \infty$  limit (right panels in Figure 4).

In Table 2 the PIMC energies of these clusters at  $T = 1 \text{ K}$  are shown. We should note the high ZPE values, due to the helium marked quantum character, which count 61.4% up to 81.5% of the corresponding potential well depth for the  $\text{He}_8\text{I}_2$  and  $\text{He}_{38}\text{I}_2$  clusters, respectively. From CCSD(T)/ECP46MWB/AVQZ

frequency analysis calculations at the global minimum of the  $\text{He}_8\text{I}_2$  cluster we also obtained a harmonic ZPE value of  $252.37 \text{ cm}^{-1}$ , which is  $20 \text{ cm}^{-1}$  higher than the anharmonic PIMC value. However, as we will see next, the quantum ground state is not only localized in the global minimum well of these systems.

In Figure 5, classical and quantum radial and angular distributions of  $\text{He}_N\text{I}_2$ , with  $N = 8, 10, 21, 26, 32$ , and  $38$ ,

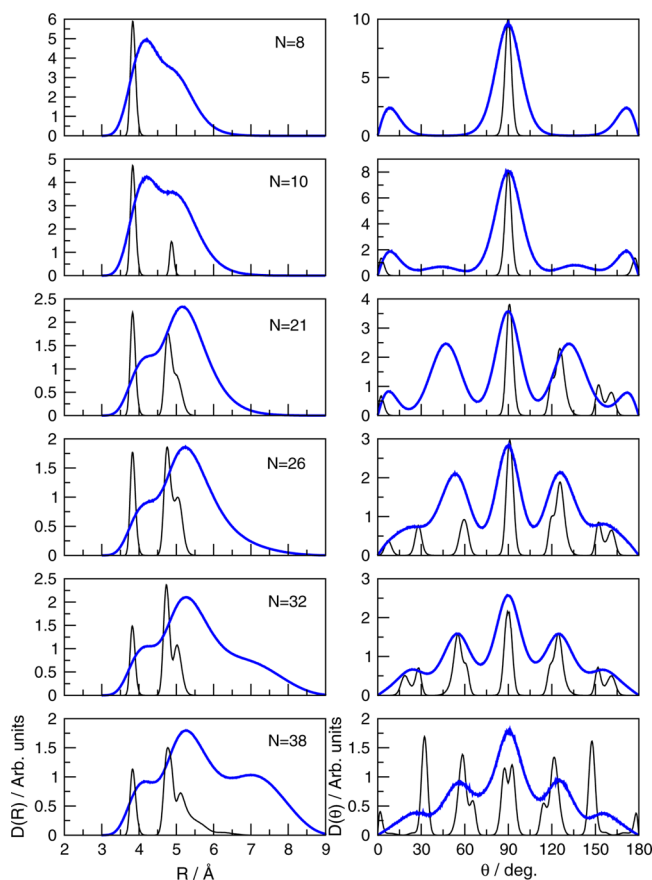


**Figure 5.** Classical (black lines) and quantum (blue/color lines) radial and angular distributions of  $\text{He}_N\text{I}_2$  clusters with  $N = 8, 10, 26, 32$ , and  $38$  at  $T = 1 \text{ K}$ .

clusters at  $T = 1 \text{ K}$  are depicted. As can be seen in the radial distributions, there are basically three main peaks. The first one is located at around  $R = 3.8 \text{ \AA}$  and corresponds to the T-shape configuration, the second one ( $R = 4.8 \text{ \AA}$ ) corresponds to the linear arrangement, and a third much broader peak appears for clusters with more than 20 He atoms around  $5 \text{ \AA}$ . This last one

**Table 2. Average Potential, Kinetic, and Total Energies Together with the Corresponding Errors Obtained from the PIMC Simulations for the Indicated  $\text{He}_N\text{I}_2$  Clusters at  $T = 1 \text{ K}^a$**

$N$	$\langle V \rangle$	$\langle K \rangle$	$\langle E \rangle$	ZPE (%)
8	$-237.54 \pm 0.08$	$93.00 \pm 0.23$	$-144.54 \pm 0.20$	230.33 (61.4)
10	$-252.60 \pm 0.14$	$101.06 \pm 0.48$	$-151.54 \pm 0.53$	314.33 (67.5)
21	$-492.89 \pm 0.37$	$229.24 \pm 0.41$	$-263.66 \pm 0.78$	720.28 (73.2)
26	$-585.85 \pm 0.58$	$295.63 \pm 0.56$	$-290.22 \pm 0.29$	916.86 (76.0)
32	$-675.74 \pm 0.45$	$366.32 \pm 0.80$	$-309.41 \pm 0.34$	1199.96 (79.5)
38	$-758.06 \pm 0.46$	$430.14 \pm 0.71$	$-327.92 \pm 0.61$	1441.74 (81.5)

<sup>a</sup>The calculated unharmonic ZPE is given, with % being the percentage with respect to the value of the corresponding potential well depth. Energies values are in  $\text{cm}^{-1}$ .

corresponds to additional rings formed in the structure, all of them with similar  $R$  distances from the  $I_2$  center of mass. The formation of these additional rings can be seen more clearly in the angular distributions. As the number of He atoms increases, the linear configuration gradually becomes more probable. Apart from the appearance of He atoms in the linear configuration, the classical calculations show us a first central ring for the  $N = 10$  cluster, a new couple of rings appear in  $N = 26$  at  $\theta = 90 \pm 30^\circ$  and finally a third couple of peaks appear at  $\theta = 90 \pm 60^\circ$  in the last case  $N = 38$ . Quantum calculations follow the same trend, with the radial peaks displaced to larger distances, and presenting a much broader profile, overlapping one another in most cases. In contrast to the classical picture, the second peak for the linear configuration is now populated even for  $N = 8$ . In turn, the angular distributions show the formation of the first shell structure at  $N = 21$ , instead of  $N = 32$  in the classical ones. Also for the  $He_{38}I_2$  cluster no peaks appear in the linear configurations, and it seems that a sort of fusion between the last couple of rings and the linear arrangement has taken place. In the quantum radial distribution for this cluster a third broad peak clearly appears at distance of 7.2 Å, indicating the formation of a second solvation shell.

In Figure 6 2D distributions are depicted. Classical ones correspond to configurations very close to those obtained by the evolutionary algorithm. At  $T = 1$  K there is not enough thermal energy for the classical He atoms to overcome the potential energy barriers between linear and T-shaped wells, which count, as we mentioned above, about  $26\text{ cm}^{-1}$ . However, the quantum calculations present a quite different scenario. The peaks that appeared in the classical calculations are now much broader and overlap with the ones corresponding to other configurations. For the larger clusters studied, a completely new shell appears, for  $N > 30$  to host the He atoms that no longer fit in the shallow minima displayed by the PES.

These 2D distributions also allow us to separate the different configurations and so perform partial integrations to quantify the He atom probability density in each of these areas. Following this idea, we divided the  $(R \cos \theta, R \sin \theta)$  plane (Figure 6) into regions corresponding to the different classical minima of the PES. In Figure 3 (right bottom panel) we display the 2D quantum distribution for the  $He_{38}I_2$  cluster by marking these spatial regions that we used to integrate over. The so-called linear one corresponds to  $R \sin \theta \leq 3$  Å, the T-shape is for  $3 \text{ \AA} \leq R \sin \theta \leq 6$  Å and  $|R \cos \theta| \leq 2$  Å, for the intermediate rings we set  $3 \text{ \AA} \leq R \sin \theta \leq 6$  Å and  $|R \cos \theta| \geq 2$  Å, whereas for the cap-like the  $R \sin \theta \geq 6$  Å area is considered. These four regions completely span the configurations space sampled in our simulations, and by partial integration over the corresponding 2D quantum distribution, we get an estimate of the number of He atoms located in those particular areas. In Table 3 the results of these partial integrations are shown for selected clusters. For  $N = 8$  there is a considerable He atom probability density at linear configurations. By integrating the T-shape (central ring structure) and the linear configuration areas separately, we conclude that roughly speaking we have 6 He atoms at the T-shape and 2 He atoms in linear configurations, each at both sides of the  $I_2$  molecule, indicating the role of the local minimum-2, just  $11.2\text{ cm}^{-1}$  higher in energy from the global minimum (Figure 2 and Table 1), in the ground vibrational quantum state of this cluster. For  $N = 10$  we find nonzero probability density at intermediate rings between the T-shape and the linear configurations. Clearly the ZPE of the He atoms is greater than the corresponding potential

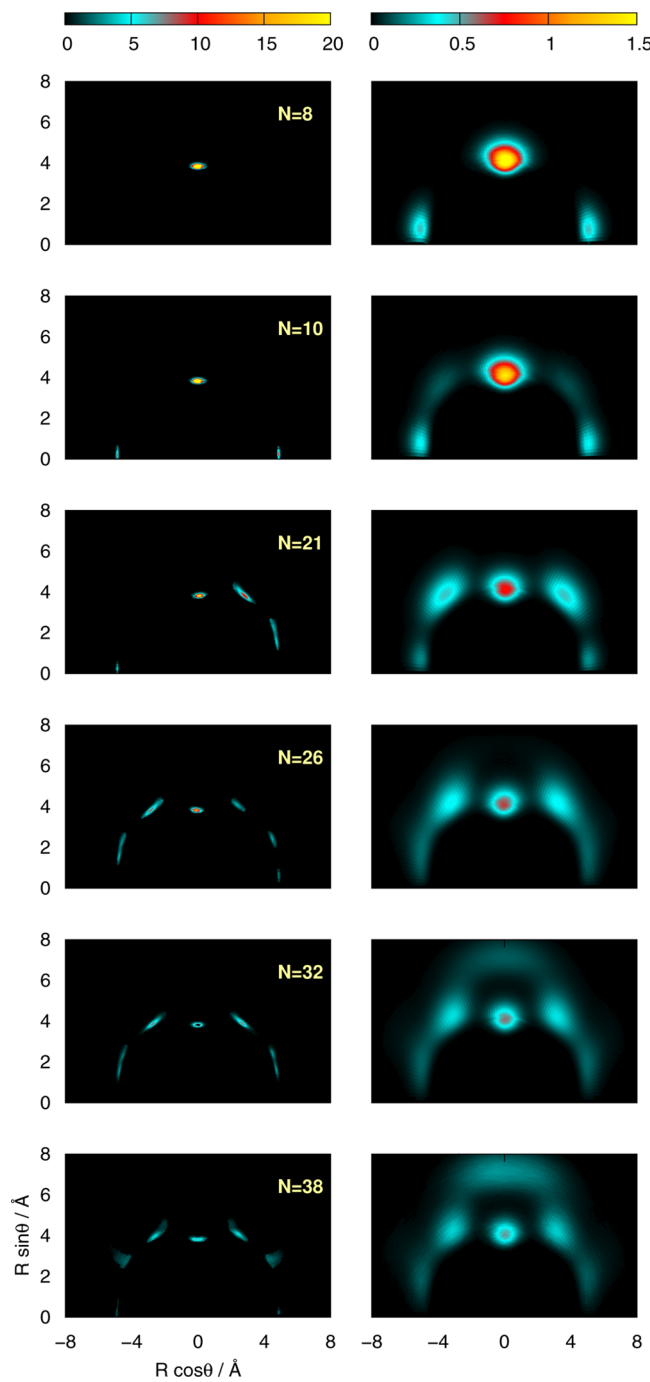


**Figure 6.** Contour plots of the classical (left panels) and quantum (right panels) distributions of the indicated  $He_N I_2$  clusters at  $T = 1$  K.

**Table 3. Partial Integration over the Quantum 2D Distributions (Also Figures 3 and 6) for the Indicated Clusters (See Text)**

$N$	linear	intermediate rings	T-shape	cap-like
8	2		6	
10	2	1.5	6.5	
21	2	12	7	
26	3.5	14.5	7	1
32	4.5	15	7	5.5
38	4.5	15.5	7	11

barriers. The T-shape configuration is soon saturated with 7 He atoms, whereas in classical results up to 10 He atoms could fit in. The linear configuration admits more than 2, but not many more. We can see that it gets saturated at less than 5 atoms. The regions near  $\theta = 60/120^\circ$  (intermediate rings) admit 15 atoms (7.5 He atoms at each side). When all these regions are completely saturated, it is the cap-like configuration that plays the role of hosting the rest of the He atoms, as we can see in Table 3 for  $N > 26$ . As an example, in Figure 3 we also show the role of the two lowest energy structures on the PES (left panels) with an energy difference between them of  $9.6 \text{ cm}^{-1}$ , on the classical and quantum 2D distributions for the  $N = 38$  cluster. The classical distribution (right top panel) seems localized at the lowest minimum energy structure (left top panels) of the cluster, whereas with zero-energy effects the local-1 minimum (left bottom panels) also contributes in the quantum-based structure.

#### IV. SUMMARY AND CONCLUSIONS

We investigated nanoscopic structures and stabilization energetics of small size  $\text{He}_N\text{I}_2$  clusters, up to  $N = 38$ . The potential surface was described fairly accurately by employing a sum-of-potentials approximation, based on *ab initio* CCSD(T)/CBS three-body parametrized  $\text{HeI}_2$  terms plus the He–He ones, to treat the full interaction within each cluster. *Ab initio* MP2 and CCSD(T) calculations were also carried out at specific geometries of selected size clusters, and the calculated interactions energies were found to be in reasonable agreement with the former analytical potential scheme.

The most stable structures for each cluster were obtained via genetic algorithm energy optimizations. We clearly see that during the initial cluster growth with  $N > 3$  the ring-like structure is slightly more favored. The completion of the first ring occurs for 8 He atoms, whereas the additional 2 He atoms, in the  $\text{He}_{10}\text{I}_2$  case, seem to prefer the linear arrangement. The following atoms in the larger clusters  $N > 12$  are forming a sort of ring structures between the central ring and linear geometries. With  $N = 21$  He atoms we observe the completion of two additional rings and the solvation in this way of the one-side I atom, whereas with  $N = 32$  we show the completion of five rings and a first solvation shell around the  $\text{I}_2$  molecule. By increasing further the number of He atoms, we found a cap-like structure for the  $\text{He}_{38}\text{I}_2$  cluster, where the He atoms start to form a second shell around the  $\text{I}_2$ .

Apart from the classical description of the energetics and spatial arrangements of the clustering process, we carried out classical MC and PIMC simulations to explicitly include thermal and nuclear quantum effects. Therefore, we determined thermal equilibrium states, ZPE values and binding energies at  $T = 1 \text{ K}$  for cluster aggregates up to  $\text{He}_{38}\text{I}_2$  one. We found that at  $T = 1 \text{ K}$  thermal effects do not alter the classical solvation behavior of  $\text{I}_2$  in the He clusters, whereas for the quantum solvated systems the interplay between the various anisotropies of the potential energy surfaces allows one to explain several details of the microscopic behavior of such doped clusters. By analyzing the corresponding radial and angular distributions, we show that the quantum delocalization is important for these small size  $\text{He}_N\text{I}_2$  systems. In the quantum case, the thermal ZPE of the He atoms is larger than the potential barriers between different minima on the PES, and thus the first shell solvation based on the partial integrations of the distributions appears at  $N = 21$ , whereas the second one starts at  $N = 26$ .

For an overall picture of the He atoms structuring around a heavy  $\text{I}_2$  dopant, we show that quantum-mechanical nature treatments should be employed. The anisotropy of the underlying PES is reflected in the solvation structure, and such information could serve for describing the transition from a molecular aggregate to a dissolved molecule, as well as for modeling superfluid effects behavior in finite-sized systems.

#### ■ AUTHOR INFORMATION

##### Corresponding Author

\*R. Prosmitti: e-mail, rita@iff.csic.es.

##### Present Addresses

<sup>†</sup>Lehrstuhl für Theoretische Chemie NC 03/52 Ruhr-Universität Bochum, D-44780 Bochum, Germany.

<sup>‡</sup>Departamento de Química, Universidade de Coimbra, 3004-535 Coimbra, Portugal.

<sup>§</sup>Grupo de Física Atómica y Molecular, Instituto de Física, Universidad de Antioquia UdeA, Calle 70 No. 52-21, Medellín, Colombia.

##### Notes

The authors declare no competing financial interest.

#### ■ ACKNOWLEDGMENTS

The authors thank to Centro de Calculo (IFF), CTI (CSIC), and CESGA for allocation of computer time. This work has been supported by MICINN grant No. FIS2011-29596-C02-01, and COST Action CM1002 (CODECS) and CM1204 (XLIC).

#### ■ REFERENCES

- (1) Sharfin, W.; Johnson, K. E.; Wharton, L.; Levy, D. H. Energy distribution in the photodissociation products of van der waals molecules: Iodine–Helium complexes. *J. Chem. Phys.* **1979**, *71*, 1292–1299.
- (2) Johnson, K. E.; Sharfin, W.; Levy, D. H. The photodissociation of van der waals molecules: Complexes of Iodine, Argon, and Helium. *J. Chem. Phys.* **1981**, *74*, 163–170.
- (3) Drobis, J. C.; Lester, M. I. Optical-optical double resonance of the  $\text{Icl}-\text{ne}$  complex: Binding energies in the  $\text{E}(0^+)$ ,  $\text{P}({}^3\Pi_1)$ , and  $\text{X}({}^1\Sigma_+)$  states. *J. Chem. Phys.* **1987**, *86*, 1662–1669.
- (4) Gutmann, M.; Willberg, D. M.; Zewail, A. H. Real-time dynamics of clusters. iii.  $\text{I}_2\text{Ne}_n$  ( $n=2-4$ ), picosecond fragmentation, and evaporation. *J. Chem. Phys.* **1992**, *97*, 8048–8059.
- (5) Rohrbacher, A.; Halberstadt, N.; Janda, K. C. The dynamics of noble gas–halogen molecules and clusters. *Annu. Rev. Phys. Chem.* **2000**, *51*, 405–433.
- (6) Boucher, D. S.; Darr, J. P.; Strasfeld, D. B.; Loomis, R. A. Spectroscopic identification of higher-order rare gas-dihalogen complexes with different geometries:  $\text{He}_{2,3}\text{Br}_2$  and  $\text{He}_{2,3}\text{ICl}$ . *J. Phys. Chem. A* **2008**, *112*, 13393–13401.
- (7) Pio, J. M.; Taylor, M. A.; van der Veer, W. E.; Bieler, C. R.; Cabrera, J. A.; Janda, K. C. Real-time dissociation dynamics of the  $\text{Ne}_2\text{Br}_2$  van der waals complex. *J. Chem. Phys.* **2010**, *133*, 014305.
- (8) Boucher, D. S.; Bradke, M. D.; Darr, J. P.; Loomis, R. A. Preferential stabilization of different isomers of weakly bound complexes. *J. Phys. Chem. A* **2003**, *107*, 6901–6904.
- (9) Buchachenko, A. A.; Prosmitti, R.; Cunha, C.; Delgado-Barrio, G.; Villarreal, P.  $\text{He}^{79}\text{Br}_2$ ,  $B_v = 8 \leftarrow X, v'' = 0$  excitation spectrum: Ab initio prediction and spectroscopic manifestation of a linear isomer. *J. Chem. Phys.* **2002**, *117*, 6117–6120.
- (10) Boucher, D. S.; Strasfeld, D. B.; Loomis, R. A.; Herbert, J. M.; Ray, S. E.; McCoy, A. B. Stabilization and rovibronic spectra of the T-shaped and linear ground-state conformers of a weakly bound rare-gas–homonuclear dihalogen complex:  $\text{HeBr}_2$ . *J. Chem. Phys.* **2005**, *123*, 104312.

- (11) Ray, S. E.; McCoy, A. B.; Glennon, J. J.; Darr, J. P.; Fesser, E. J.; Lancaster, J. R.; Loomis, R. A. Experimental and theoretical investigations of the  $\text{HeI}_2$  rovibronic spectra in the  $\text{I}_2$  B-X, 20-0 region. *J. Chem. Phys.* **2006**, *125*, 164314.
- (12) Valdés, A.; Prosmitti, R.; Villarreal, P.; Delgado-Barrio, G.; Lemoine, D.; Lepetit, B. Ab initio vibrational predissociation dynamics of  $\text{He}-\text{I}_2(\text{B})$  complex. *J. Chem. Phys.* **2007**, *126*, 244314.
- (13) García-Gutiérrez, L.; Delgado-Tellez, L.; Valdés, A.; Prosmitti, R.; Villarreal, P.; Delgado-Barrio, G. Intermolecular ab initio potential and spectroscopy of the ground state of  $\text{HeI}_2$  complex revisited. *J. Phys. Chem. A* **2009**, *113*, 5754-5762.
- (14) Valdés, A.; Prosmitti, R.; Villarreal, P.; Delgado-Barrio, G. Ab initio calculations, potential representation and vibrational dynamics of  $\text{He}_2\text{Br}_2$  van der waals complex. *J. Chem. Phys.* **2005**, *122*, 044305-1-8.
- (15) Valdés, A.; Prosmitti, R.; Villarreal, P.; Delgado-Barrio, G. A theoretical study of  $\text{He}_2\text{ICl}$  van der waals cluster. *J. Chem. Phys.* **2006**, *125*, 014313.
- (16) Valdés, A.; Prosmitti, R.; Villarreal, P.; Delgado-Barrio, G.; Werner, H.-J. Ab initio potential energy surface and spectrum of the  $\text{B}^{\langle 3 \rangle \Pi}$  state of the  $\text{HeI}_2$  complex. *J. Chem. Phys.* **2007**, *126*, 204301.
- (17) Delgado-Tellez, L.; Valdés, A.; Prosmitti, R.; Villarreal, P.; Delgado-Barrio, G. Ab initio characterization of the  $\text{Ne}-\text{I}_2$  van der waals complex: Intermolecular potentials and vibrational bound states. *J. Chem. Phys.* **2011**, *134*, 214304.
- (18) Prosmitti, R.; Cunha, C.; Buchachenko, A. A.; Delgado-Barrio, G.; Villarreal, P. Vibrational predissociation of  $\text{NeBr}_2$  ( $X, v=1$ ) using an ab initio potential energy surface. *J. Chem. Phys.* **2002**, *117*, 10019-10025.
- (19) Pio, J. M.; van der Veer, W. E.; Bieler, C. R.; Janda, K. C. Product state resolved excitation spectroscopy of  $\text{He}-$ ,  $\text{Ne}-$ , and  $\text{Ar}-\text{Br}_2$  linear isomers: Experiment and theory. *J. Chem. Phys.* **2008**, *128*, 134311.
- (20) Grebenev, S.; Toennies, J. P.; Vilessov, A. F. Superfluidity within a small Helium-4 cluster: The microscopic Andronikashvili experiment. *Science* **1998**, *279*, 2083-2086.
- (21) Nauta, K.; Miller, R. E. Formation of cyclic water hexamer in liquid helium: The smallest piece of ice. *Science* **2000**, *287*, 293-295.
- (22) Callegari, C.; Lehmann, K. K.; Schmied, R.; Scoles, G. Helium nanodroplet isolation rovibrational spectroscopy: Methods and recent results. *J. Chem. Phys.* **2001**, *115*, 10090-10110.
- (23) Toennies, J. P.; Vilessov, A. F. Superfluid helium droplets: A uniquely cold nanomatrix for molecules and molecular complexes. *Angew. Chem., Int. Ed.* **2004**, *43*, 2622-2648.
- (24) Echt, O.; Mark, T. D.; Scheier, P. *Handbook of Nanophysics, Vol. 2: Clusters and Fullerenes*; CRC Press, Taylor and Francis Group: Boca Raton, FL, 2010.
- (25) de Lara-Castells, M. P.; Prosmitti, R.; Delgado-Barrio, G.; López-Durán, D.; Villarreal, P.; Gianturco, F. A.; Jellinek, J. Polar di-halogen molecules solvated in bosonic helium clusters: The paradigm of  $\text{ICl}(X)$ . *Phys. Rev. A* **2006**, *74*, 053201.
- (26) Zillich, R. E.; Whaley, K. B. Solvation structure and rotational dynamics of  $\text{LiH}$  in  ${}^4\text{He}$  clusters. *J. Phys. Chem. A* **2007**, *111*, 7489-7498.
- (27) Marinetti, F.; Bodo, E.; Gianturco, F. A. Microsolvation of an ionic dopant in small  ${}^4\text{He}$  clusters:  $\text{OH}({}^3\Sigma)^{({}^4\text{He})_n}$  via genetic algorithm optimizations. *ChemPhysChem* **2007**, *8*, 93-100.
- (28) Ramílowski, J. A.; Mikosz, A. A.; Farrelly, D.; Cagide-Fajn, J. L.; Fernández, B. Rotational structure of small  ${}^4\text{He}$  clusters seeded with HF, HCl, and HBr molecules. *J. Phys. Chem. A* **2007**, *111*, 12275-12288.
- (29) Bonhommeau, D.; Lewerenz, M.; Halberstadt, N. Fragmentation of ionized doped helium nanodroplets: Theoretical evidence for a dopant ejection mechanism. *J. Chem. Phys.* **2008**, *128*, 054302-1-18.
- (30) Li, H.; Blinov, N.; Roy, P.-N.; Le Roy, R. J. Path-integral Monte Carlo simulation of 3 vibrational shifts for  $\text{CO}_2$  in  $(\text{He})_n$  clusters critically tests the  $\text{HeCO}_2$  potential energy surface. *J. Chem. Phys.* **2009**, *130*, 144305-1-11.
- (31) Guillou, G.; Zanchet, A.; Leino, M.; Viel, A.; Zillich, R. E. Theoretical study of  $\text{Rb}_2$  in  $\text{He}_n$ : Potential energy surface and Monte Carlo simulations. *J. Phys. Chem. A* **2011**, *115*, 6918-6926.
- (32) Rodríguez-Cantano, R.; Pérez de Tudela, R.; López-Durán, D.; González-Lezana, T.; Gianturco, F. A.; Delgado-Barrio, G.; Villarreal, P. Quantum rotation of  $\text{Rb}_2$  ( ${}^3\Sigma_u^+$ ) attached to  $\text{He}_n$  droplets: a path-integral Monte Carlo study. *Eur. Phys. J. D* **2013**, *67*, 1-7.
- (33) Valdés, A.; Barragán, P.; Pérez de Tudela, R.; Medina, J. S.; Delgado-Tellez, L.; Prosmitti, R. A theoretical study of multiple isomers of the  $\text{He}_2\text{I}_2$  complex. *Chem. Phys.* **2012**, *399*, 39-45.
- (34) Valdés, A.; Prosmitti, R.; Villarreal, P.; Delgado-Barrio, G. Theoretical characterization of intermolecular vibrational states through the multi-configuration time dependent hartree approach: The  $\text{He}_{2,3}\text{ICl}$  clusters. *J. Chem. Phys.* **2011**, *135*, 244309-1-9.
- (35) Valdés, A.; Prosmitti, R. Quantum mechanical characterization of the  $\text{He}_4\text{ICl}$  weakly bound complex. *J. Phys. Chem. A* **2013**, *117*, 7217-7223.
- (36) Aziz, R. A.; Slaman, M. J. An examination of ab initio results for the helium potential energy curve. *J. Chem. Phys.* **1991**, *94*, 8047-8053.
- (37) Martin, J. M. L.; Sundermann, M. Correlation consistent valence basis sets for use with the stuttgartdresdenbonn relativistic effective core potentials: The atoms Ga-Kr and In-Xe. *J. Chem. Phys.* **2001**, *114*, 3408-3420.
- (38) Woon, D. E.; Dunning, T. H., Jr. Gaussian basis sets for use in correlated molecular calculations. IV. Calculation of static electrical response properties. *J. Chem. Phys.* **1994**, *100*, 2975-2988.
- (39) Frisch, M. J.; et al. *Gaussian 09*, Revision D.01; Gaussian Inc.: Wallingford, CT, 2009.
- (40) Werner, H.-J.; Knowles, P. J.; Knizia, G.; Manby, F. R.; Schütz, M.; et al. *Molpro*, version 2012.1, a package of ab initio programs, 2012; see <http://www.molpro.net>.
- (41) Boys, S. F.; Bernardi, F. The calculation of small molecular interactions by the differences of separate total energies. some procedures with reduced errors. *Mol. Phys.* **1970**, *19*, 553-566.
- (42) Iwamatsu, M. Applying evolutionary programming to structural optimization of atomic clusters. *Comput. Phys. Commun.* **2001**, *142* (13), 214-218.
- (43) Feynman, R. P.; Hibbs, A. *Quantum Mechanics and Path Integrals*; McGraw Hill: New York, 1965.
- (44) Pérez de Tudela, R.; Barragán, P.; Prosmitti, R.; Villarreal, P.; Delgado-Barrio, G. Internal proton transfer and  $\text{H}_2$  rotations in the  $\text{H}_5^+$  cluster: A marked influence on its thermal equilibrium state. *J. Phys. Chem. A* **2011**, *115*, 2483-2488.
- (45) Ceperley, D. M. Path integrals in the theory of condensed helium. *Rev. Mod. Phys.* **1995**, *67*, 279-355.
- (46) Takahashi, M.; Imada, M. Monte Carlo calculation of quantum systems. ii. higher order correction. *J. Phys. Soc. Jpn.* **1984**, *53*, 3765-3769.
- (47) Sakkos, K.; Casulleras, J.; Boronat, J. High order chin actions in path integral Monte Carlo. *J. Chem. Phys.* **2009**, *130*, 204109.
- (48) Sprik, M.; Klein, M. L.; Chandler, D. Staging: A sampling technique for the Monte Carlo evaluation of path integrals. *Phys. Rev. B* **1985**, *31*, 4234-4244.
- (49) Metropolis, N.; Rosenbluth, A. W.; Rosenbluth, M. N.; Teller, A. H.; Teller, E. Equation of state calculations by fast computing machines. *J. Chem. Phys.* **1953**, *21*, 1087-1092.
- (50) Barker, J. A. A quantum-statistical Monte Carlo method; path integrals with boundary conditions. *J. Chem. Phys.* **1979**, *70*, 2914-2918.
- (51) Herman, M. F.; Bruskin, E. J.; Berne, B. J. On path integral Monte Carlo simulations. *J. Chem. Phys.* **1982**, *76*, 5150-5155.